RPE | Radiation Physics & Engineering
A Peer-Reviewed Journal
Published by K.N. Toosi University of Technology
http://rpe.kntu.ac.ir
Research Article

Radiation Physics and Engineering 2023; 4(3):65–72

Secondary particle dose assessment during the proton therapy of liver cancer: A Monte Carlo study

Leyli Mogheiseh[a], Ali Asghar Mowlavi[b], Sayyed Bijan Jia[c], Reza Shamsabadi[a,*]

[a] *Physics Department, Hakim Sabzevari University, Sabzevar, Iran*
[b] *Physics Department, Ferdowsi University, Mashhad, Iran*
[c] *Physics Department, University of Bojnord, Bojnord, Iran*

HIGHLIGHTS

- The absorbed dose of secondary particles in proton therapy of liver cancer was assessed.
- A simplified MC model of MIRD-UF standard phantom was simulated using MCNPX.
- The absorbed doses were assessed for 90 MeV and 120 MeV of primary proton beams.
- The fluence of internal secondary particles doses was considerably small.
- The most contribution of the secondary particle doses was absorbed inside the liver tissue.

ABSTRACT

Proton therapy of liver tumors can be challenging due to the absorbed dose of produced secondary particles in non-target organs. This study aims to evaluate the absorbed dose of secondary particles during the proton therapy of liver cancer through the MCNPX Monte Carlo (MC) code by a simplified MIRD-UF standard phantom. At first, a simplified MC model of MIRD-UF standard phantom was simulated using MCNPX. After the proper proton energies calculation ranging from 90 to 120 MeV for $4 \times 4 \times 4$ cm^3 tumor irradiation, mesh tally type 3 and F6 tally were used to calculate the depth dose profiles as well as the absorbed dose of protons and secondary particles in non-involved organs. The obtained results illustrated that the fluence of internal secondary particles doses was considerably small in comparison with primary protons. Furthermore, most of neutrons and photons doses were absorbed around the liver tissue for all performed proton energies (i.e. 90 and 120 MeV) which non-target organs did not receive a significant high dose. Furthermore, the absorbed dose of secondary photons and neutrons had slight variations in considered normal tissues near the liver. The calculated results in this study indicated that during the proton therapy of liver cancer, the most contribution of the secondary particle doses was absorbed inside the liver tissue. Hence, it can be expected the probable side effects (secondary cancers) associated with the liver cancer proton therapy may be decreased however, the presence of secondary particles should not be ignored.

KEYWORDS

Liver cancer
Proton therapy
Secondary particles
Monte Carlo simulation
Non-involved organs

HISTORY

Received: 28 March 2023
Revised: 26 April 2023
Accepted: 5 May 2023
Published: Summer 2023

1 Introduction

Liver cancer is one of the most common causes of cancer related-death worldwide which about 780,000 death cases were reported in 2018 (Keane et al., 2016; Bray et al., 2018). For liver cancer treatment, various modalities including surgery, chemotherapy, and radiotherapy (RT) have been proposed. Radiotherapy is a critical treatment method which can be applied for different stages of liver cancer (Chen et al., 2018). Recent developments in radiotherapy techniques have increased the safety and accuracy of liver cancer treatment (Dionisi et al., 2021).

RT via proton pencil beam has become as one of the most attractive modalities for the liver cancer treatment which can lead to promising clinical outcomes. Due to the unique physical properties of the proton beam like finite range of energy deposition, RT with the proton pencil beam has dosimetric advantages compared with X-ray therapy (Gandhi et al., 2015; Wang et al., 2008; Chuong

*Corresponding author: R.shamsabadi@hsu.ac.ir

https://doi.org/10.22034/rpe.2023.391186.1126
https://dorl.net/dor/20.1001.1.26456397.2023.4.3.8.6

et al., 2020). Since most of the proton energy can be delivered near the end of beam paths (so-called as the Bragg peak), secondary cancers and damages to the healthy surrounding tissues would be reduced. Nevertheless, due to the presence of critical organs such as kidneys, small intestine, heart, lungs, and spinal cord in the proton path, proton therapy of liver tumors must be carefully employed (Wang et al., 2008; Chen et al., 2018; Doyen et al., 2016).

Due to the different proton interactions within tissues including coulomb interaction with atomic electrons and elastic nuclear scattering, different secondary particles such as photons, secondary protons, neutrons, and deuterons can be produced (Kraft, 2000). It is worth mentioning that photons and neutrons are the most commonly created secondary particles during the proton therapy (Jarlskog et al., 2008). However, these created secondary particles have little impact on the Bragg peak, secondary particles may have large linear energy transfer (LET) values and thus influence the absorbed dose of healthy organs. In this regard the risk of radiation-induced secondary cancers may be increased (Taddei et al., 2009; Jiang et al., 2005). So, the risk of secondary cancers should be considered during proton therapy to improve the treatment outcomes.

Evaluation of the absorbed doses caused by non-primary particles during the proton therapy has been discussed in the previously published literatures (Brenner and Hall, 2008; Brenner et al., 2009). The contribution of secondary neutrons based on the various parameters including aperture size, proton range, and proton scanning area in a uniform scanning system have experimentally measured by Zheng et al. (Zheng et al., 2012). In this study minimizing the beam scanning area showed that the equivalent neutron dose for uniform scanning beams could be decreased.

The absorbed dose of neutron and photon secondary particles during the proton therapy of the human brain was estimated by Jia et al. (Jia et al., 2014). The obtained results showed that for high-energy proton beams the amount of escaped energies by secondary neutrons raised about ten times rather than secondary photons. Moreover, the absorbed dose of secondary particles in non-involved organs was studied by Ahmadi Ganjeh et al. (Ahmadi Ganjeh et al., 2019), through the simulation of a typical liver tumor in a human ORNL-MIRD phantom. The obtained results indicated that the close organs to the liver received a higher dose values than the other organs while the absorbed dose of secondary particles in out-of-filed organs was slight.

Despite the low absorbed dose of created secondary particles within the out-of-field organs, the risk of secondary cancers induction might be a concern (Paganetti, 2002). Since, primary cancer treatment by proton therapy may increase the risk of radiation-induced secondary malignancies inside the out of radiation field organs (Xu et al., 2008; Kry et al., 2017; Howell, 2012), the current study aims to evaluate the absorbed dose of secondary particles in different normal organs near the target volume (liver tissue) through the simulation of the ORNL-MIRD phantom by the MCNPX Monte Carlo code.

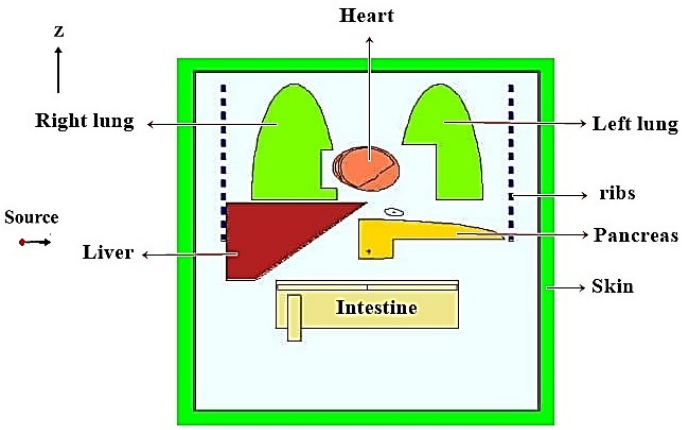

Figure 1: The simulated model of simplified MIRD-UF standard phantom as well as the proton source.

2 Material and Methods

As mentioned previously, this study aimed to evaluate the absorbed dose of secondary particles in different normal organs in the vicinity of the liver tissue through the proton beams treatment. To doing so, a simplified MIRD-UF standard phantom was modeled using MCNPX MC code version 2.6. Different organs such as ribs, lungs, kidneys, heart, intestine, skin, and liver were simulated. It should be mentioned that to simulate the considered phantom, all geometry details have been exactly extracted from the MIRD-UF standard phantom (Snyder et al., 1969). The primary proton source was mono-energetic point source which was located 30.1 cm far from the center of irradiated volume (liver tissue). Furthermore, all simulations were performed in the CPU Intel Core i7/8 GB RAM computing system. The simulated MC model of considered phantom as well as the primary proton source have displayed in Figure1.

To evaluate the absorbed dose of secondary particles in close healthy organs, a hypothetical tumor with dimensions of about $4 \times 4 \times 4$ cm^3 (about 35% of liver tissue in MIRD-UF standard phantom) was also simulated inside the liver tissue. The elemental compositions of the considered tumor are reported in Table 1.

To obtain the appropriate proton energy beams which cover entirely the considered tumor, mono-energetic proton beams were simulated at the right part of the body (indicated in Fig. 1) with 2.5 MeV increment steps, ranging from 90 to 120 MeV. In all simulation procedures, the energy cut-off for photons and protons were set equal to 1 keV and 1 MeV, respectively. While the particle energy falls below the considered cut-off value, the particle transportation is terminated and its remaining energy deposited locally. It should be mentioned that to reach a minimal statistical error of about 0.1%, 50 million primary particles were transported.

Mesh tally type 3 was utilized to calculate the averaged energy deposition over the volume. To convert these values into the absorbed dose, the results were divided by the organ densities. Furthermore, to evaluate the mean

Table 1: Elemental fractions (by weight percentage) of simulated liver tissue in present study.

	Elemental weight fractions (%)								
	H	C	N	O	P	S	K	Na	Cl
Liver tissue	10.3	18.6	2.8	67.1	0.2	0.3	0.3	0.2	0.2

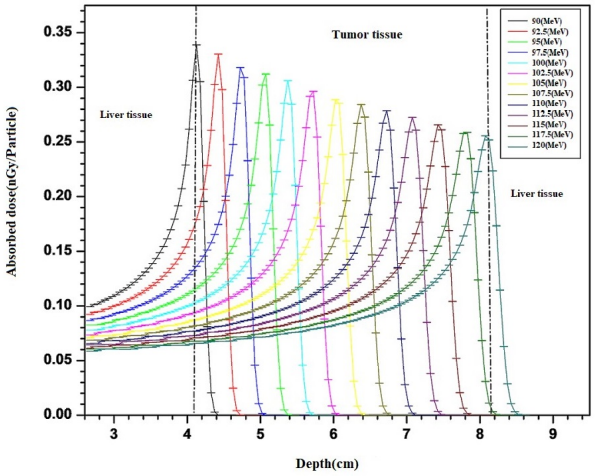

Figure 2: The depth dose profiles inside the simulated phantom for the incident proton beams with the energies ranging from 90 to 120 MeV.

absorbed dose in each organ, the F6 tally was performed. The F6 tally card gives the energy deposition in terms of a mega-electron volt (MeV) per gram inside the whole-organ. The 3-dimensional (3D) fluences of secondary particles for mono-energetic proton beams were calculated to assess the effect of these secondary particles on the absorbed dose of normal tissues (mentioned organs). Finally, the energy spectra of photon and neutron secondary particles were determined.

3 Results and discussion

The calculated results of depth dose profiles for various mono-energetic proton beams ranging from 90 to 120 MeV with 2.5 MeV increment steps inside the simulated phantom have illustrated in Fig. 2.

The appropriate energy range for the treatment of any tumor depends on the thickness and the tumor site which is located in front of the beam. As displayed in Fig. 2, the position of the Bragg peaks corresponding to the mono-energetic proton beams ranging from 90 MeV to 120 MeV fall inside the considered tumor. While increasing the proton energy, the maximum absorbed dose in the irradiated target region has decreased in which low energy protons have narrower Bragg peaks and higher heights as well. This issue can be justified by the fact that the penetration of proton beam inside the liver tissue increases with the proton energy increment. Hence, due to the increasing the interactions by the proton energy increment, the height of the Bragg peaks has decreased.

The only noticeable difference in Fig. 2, is the width distribution of the simulated Bragg peaks. The total area attributed to each obtained Bragg peak is the same for all energies, while increasing the proton beam energies, corresponding Bragg peak becomes shorter and wider which is with the agreement of the calculated results by Jia et al. in the treatment of brain tumors through proton beams (Jia et al., 2014).

As mentioned earlier, protons and other charged particles lose their energy through the inelastic interactions with atomic electrons and nuclei which consequently can lead to the production of secondary particles such as photons and neutrons. The produced photons and neutrons can travel to the far distances and deposit their energy in various organs either close or far distance to the target volume. Hence, production of the secondary particles through the interaction of the proton beam with liver tissue may impact the absorbed dose inside the surrounding organs.

The depth dose profiles of the secondary neutrons, photons, as well as the total depth dose profile per incident primary proton beam with the energy of 120 MeV have depicted in Fig. 3.

As depicted in Fig. 3, the absorbed dose of primary protons is the dominant dose distribution in the liver tissue. This finding can be due to the fact that most of primary protons with considered energy in this study, loss their energy inside the liver tissue and consequently influence the delivered dose to the target region. The comparison of the neutron and photon dose profiles indicates that the absorbed dose associated with the neutrons secondary particles is greater than ones calculated for the photons in all depths within the liver. The energy deposition of secondary neutrons and photons, produced in human brain proton therapy have been evaluated by the Jia et al. (Jia et al., 2014). The obtained results of this study showed that for high energy proton beams, the amount of escaped energy by neutrons was almost 10 times larger than that

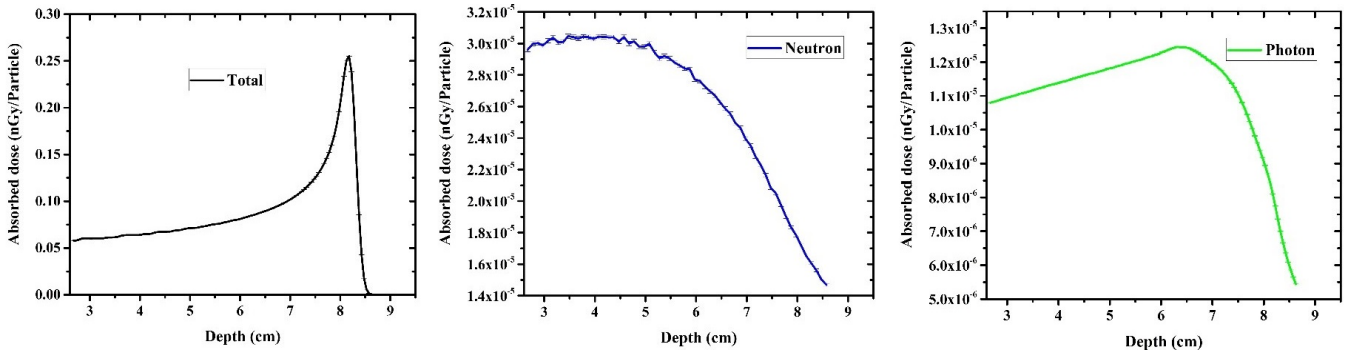

Figure 3: The depth dose profiles of all primary and secondary simulated particles (left panel), neutrons (middle panel), and photons (right panel) for 120 MeV proton beam.

by photons which is with the agreement of calculated results in present study.

The absorbed dose of secondary neutrons and photons per 1 Gy therapeutic dose in the liver and the surrounding normal organs for 120 MeV and 90 MeV proton energies have been plotted in Figs. 4 and 5, respectively.

With the comparison of Figs. 4 and 5, it can be concluded that secondary neutrons dose contribution was higher than ones for secondary photons inside all considered organs. As illustrated in Figs. 4 and 5, it can be seen that the most absorbed dose of secondary particles was scored in the irradiated target region (simulated tumor) for all performed proton energies (i.e., 90 MeV and 120 MeV). Furthermore, it is evident that the absorbed dose of secondary photons and neutrons have slight variations in the near healthy tissues to the liver. As illustrated in Figures 4 and 5, the amount of absorbed dose in kidneys and gallbladder, due to their proximity to the considered tumor tissue, were more than those absorbed inside the other considered organs.

The calculated total absorbed dose inside the considered organs at risk for 50 Gy prescribed dose and 120 MeV primary proton energy, have been reported in Table 2.

As reported in Table 2, the calculated total absorbed dose for 120 MeV primary protons and 50 Gy prescribed dose within the liver tissue is greater than those calculated for other organs. In fact, most of particle doses have been absorbed within the liver. Besides the liver, due to the Gallbladder location in human body has received the high dose radiation.

Table 2: The total absorbed dose within the non-involved organs during the proton therapy of liver cancer for 120 MeV primary proton beam and 50 Gy prescribed dose.

Organ	Absorbed dose (Gy)
Left lung	2.30 ± 0.12
Right lung	5.78 ± 0.13
Heart wall	4.70 ± 0.12
Heart	4.55 ± 0.11
liver	51.8 ± 1.20
Right kidney	2.08 ± 0.09
Left kidney	7.77 ± 0.15
Gallbladder	16.30 ± 0.36
Pancreases	8.42 ± 0.24
Spleen	3.66 ± 0.07

The energy spectra associated with photon and neutron secondary particles for 100 MeV proton energy per one incident proton beam have been illustrated in Fig. 6.

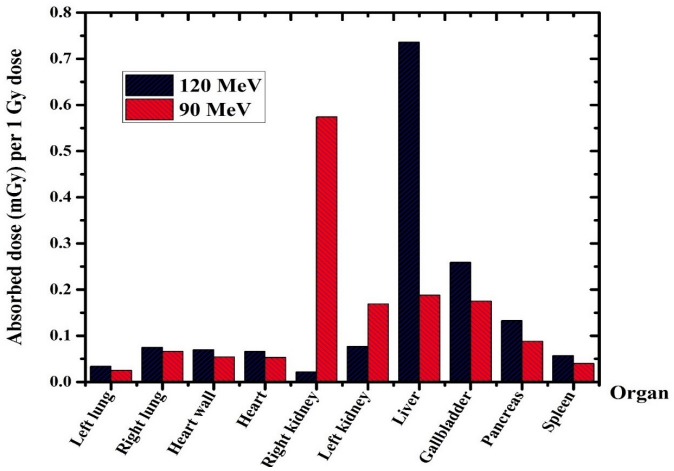

Figure 4: The neutron absorbed dose per 1 Gy therapeutic dose in the liver and the non-target organs for proton energies of 120 MeV and 90 MeV.

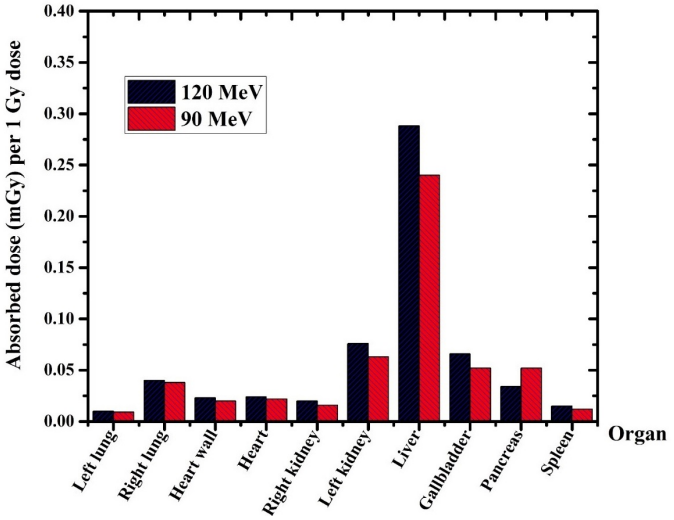

Figure 5: The photon absorbed dose per 1 Gy therapeutic dose within the liver and non-target organs for proton energies of 90 MeV and 120 MeV.

Table 3: The absorbed dose of primary and created secondary particles at a specific depth of 8.175 cm per incident primary proton beam.

Total absorbed dose (nGy)	Proton absorbed dose (nGy)	Neutron absorbed dose (nGy)	Photon absorbed dose (nGy)
$0.2552 \pm 7.6 \times 10^{-3}$	$0.2551 \pm 2.6 \times 10^{-3}$	$1.65 \pm 4.95 \times 10^{-6}$	$8.165 \pm 2.43 \times 10^{-6}$

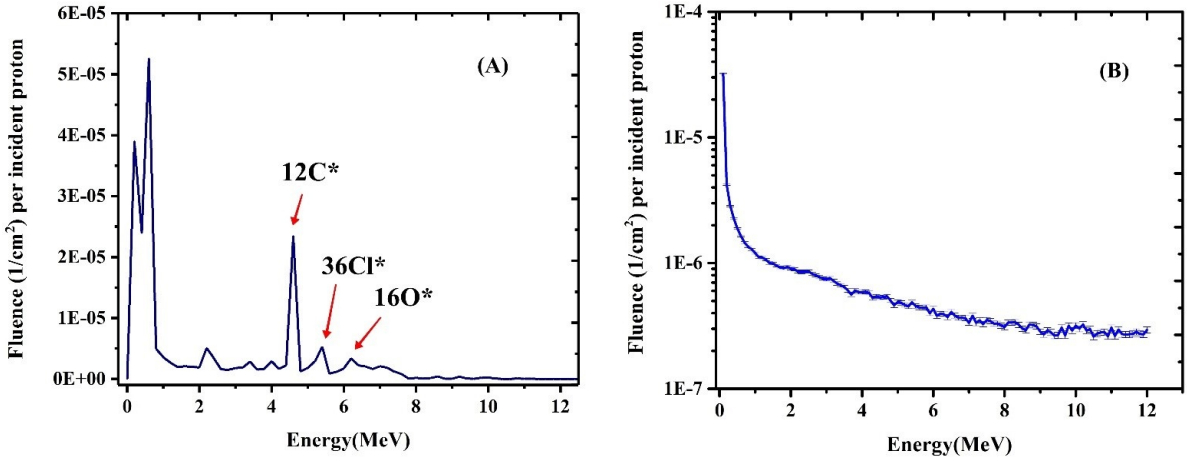

Figure 6: The secondary particle energy spectra of A) photons and B) neutrons produced by 100 MeV incident primary proton beam.

The observed sharp peaks in the energy spectrum (Fig. 6-A) are the characteristic photon energies which can be linked to the characteristic gamma-ray energies emitted from the C-12, Cl-36, and O-16. As demonstrated by Fig. 6-A, the first highest peak is related to the electron-positron annihilation which results in the release of the energy of about 1.22 MeV. The second highest sharp peak in Fig. 6-A, appears at about 4.5 MeV which is related to the excited C-12 nucleus. The calculated highest peak of photon energy spectrum (C-12) is in accordance with the reported value by previously published literature (Polf et al., 2009). The calculated C-12 characteristic gamma-ray energy by Hashemi et al. (Hashemi et al., 2020), was about 4.42 MeV. The observed difference can be related to the applied MC code and different simulated tissues. The other sharp peaks at the energies of 5.26 and 6.2 MeV are relevant to the Cl-36 and O-16. Furthermore, the maximum variations of the photon energy spectrum have appeared below 10 MeV which can be justified by the fact that the maximum non-elastic nuclear cross-section arises at the energies of about 10 to 50 MeV (Malmer, 2001).

As shown in Fig. 6-B, the neutron energy spectrum has a peak at the low-energy region which decrease by energy increment. Highest fluence in the low energy part of neutron spectrum can be related to slow neutrons which their contribution decrease by the neutron energy increment.

The total absorbed dose as well as the absorbed dose of primary and secondary particles at a specific depth of 8.175 cm inside the liver tissue are reported in Table 3.

The reported total absorbed doses of simulated particles in Table 3, demonstrated that the absorbed dose of secondary particles had a negligible impact than those obtained for primary protons. Moreover, the absorbed dose of photons was 4.9 times bigger than neutron at the fixed depth in liver tissue.

The 2-dimensional (2D) distributions of the neutron and photon fluences, corresponding to the 120 MeV proton beam energy outside the liver tissue (superior and inferior of the liver) are plotted at $Z = 24$ cm and 46 cm in Figs. 7 and 8, respectively.

The 2D distributions of the neutrons and photons fluence in Figs. 7 and 8 showed that created secondary particles have a minimal influence to the absorbed dose within the surrounding normal organs which the absorbed dose values within the surrounding tissues can be decreased by increasing the lateral distances. As shown in Fig. 7, the contribution of photons was higher than that for neutrons. Moreover, the same approach can be seen in Fig. 8, which can be concluded that minimum dose has been absorbed by neutrons in healthy tissues. The small contribution of the secondary particles depth-dose values beyond the considered tumor size (in Figs. 7 and 8), can be related to the stray and leakaged particles to other healthy organs. Scattered secondary neutrons can travel far distances from the irradiated volume which can lead to a whole body neutron dose exposure (Hälg and Schneider, 2020).

The 2D distributions of the neutron and photon fluences, corresponding to the 120 MeV proton beam energy inside the liver are plotted at $Z = 36$ cm in Fig. 9.

Plotted results in Fig. 9 indicated that most of the secondary particles (neutrons and photons) have been created inside the irradiated liver tissue. So, a large amount of the secondary particles doses delivered inside the liver tissue and secondary particles had little impact on the absorbed dose of surrounding healthy organs. Since these created secondary particles during the proton therapy release a large amount of their energy before reaching to the tumor, despite the small amount of the absorbed dose corresponding to the secondary particles in non-involved organs as well as consequent side effects, this small fraction

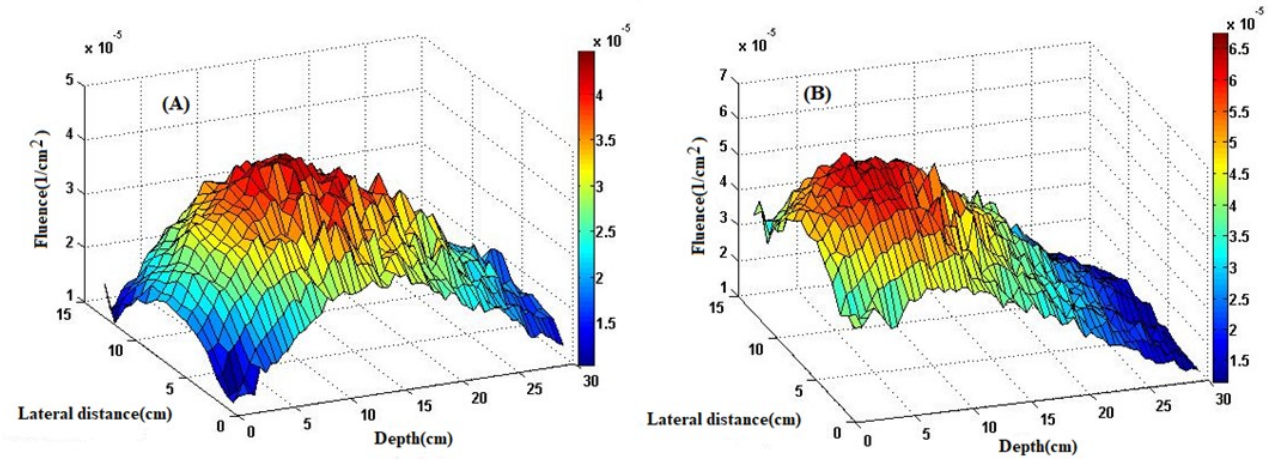

Figure 7: The 2D fluence distributions of A) neutrons and B) photons secondary particles at $Z = 24$ (at the bottom of the liver) per incident primary proton.

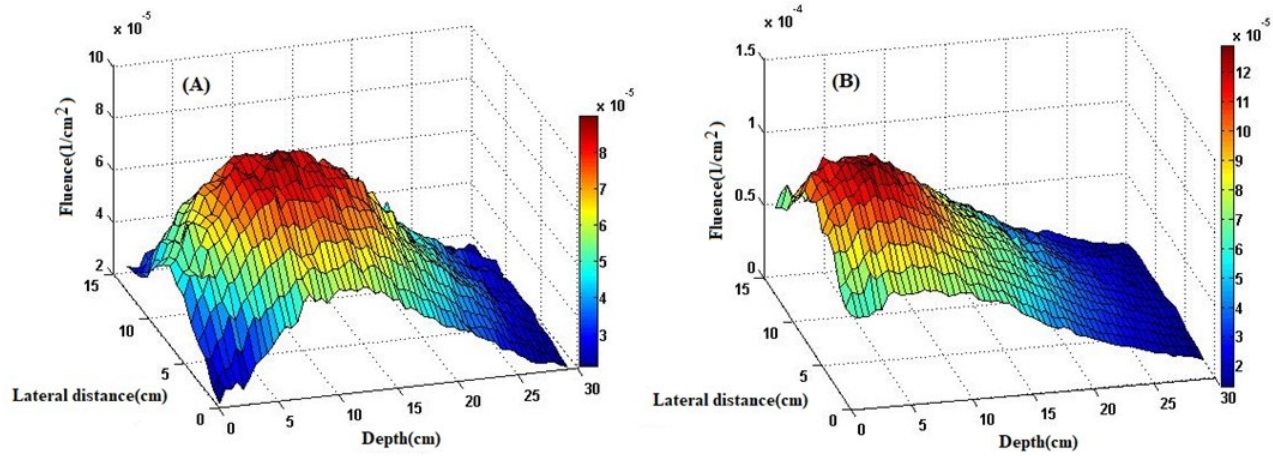

Figure 8: The 2D fluence distributions of A) neutrons and B) photons secondary particles at $Z = 46$ cm (at the above of the liver) per incident primary proton.

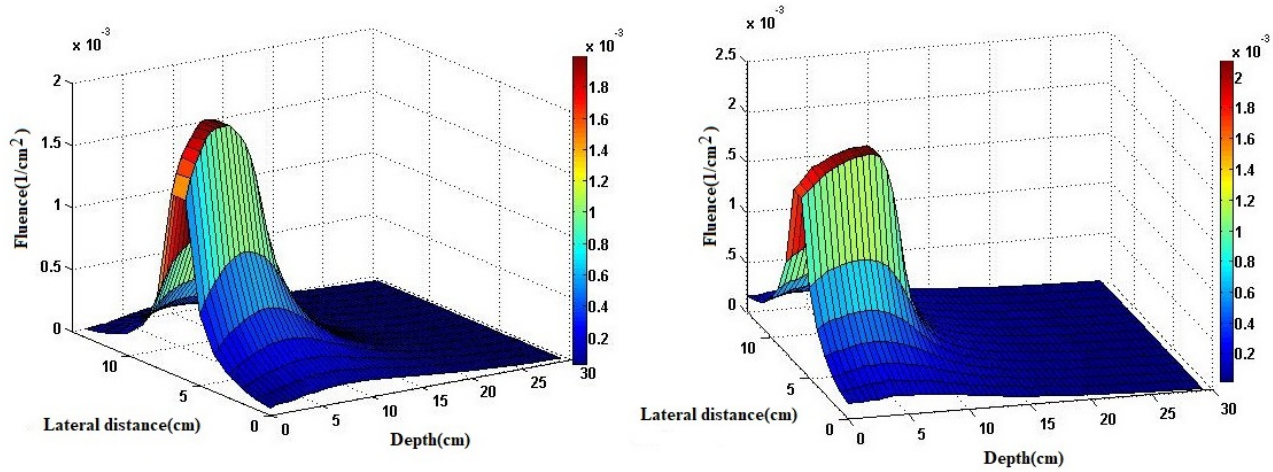

Figure 9: The 2D influence distributions of neutrons (left panel) and photons (right panel) secondary particles at $Z = 36$ cm (inside the liver tissue) per incident primary proton.

of absorbed dose in healthy tissues should not be ignored.

Despite the lower absorbed dose in proton therapy relevant to the created secondary particles, the main concern is the production of secondary neutrons which may lead to some late effects. The deposited dose by protons and secondary charged particles can be mainly delivered around the irradiated volume, whilst the scattered secondary neutrons can increase the whole-body neutron dose within the

healthy sounding organs (Hälg and Schneider, 2020).

The neutron equivalent doses under various treatment conditions have been evaluated by Zheng et al. (Zheng et al., 2012). The obtained results revealed that the neutron equivalent dose per therapeutic dose for uniform scanning beams was slightly lower than that for a passive scattering beam through the similar treatment conditions. In our present study the absorbed dose measurements related to the secondary particles during the proton therapy of liver cancer have been calculated for the minimum and maximum proton energies (90 MeV and 120 MeV in our study) to compare the contribution of the absorbed dose by secondary particles in the tumor volume and sounding healthy organs.

Totally, proton therapy technique in clinical purposes can be applied by passive scattering or active scanning methods. In passive scattering proton therapy, there are more components than in active scanning method as the beam delivery system. This issue can directly increase the neutron doses through the interaction of the primary beam with the components of the dose delivery system (Hälg and Schneider, 2020).

The main advantage of proton therapy over photon therapy is the localized dose distribution which the healthy tissues around the tumor would be minimally damaged. This feature makes proton therapy as the suitable choice for the treatment of tumors located near sensitive organs. Depending on the location of the tumor, proton therapy procedures can be designed to achieve the most optimal treatment with minimizing the absorbed dose to the normal tissues.

4 Conclusions

In this study, a simplified MIRD-UF standard phantom was modeled by MCNPX 2.6 code to evaluate the absorbed dose of secondary particles in various normal out-of-field organs through the proton therapy of liver cancer. For the selected geometry, the Bragg peaks of proton beams with the energies ranging from 90 to 120 MeV, fall inside the considered tumor. The calculated results of organs absorbed dose indicated that most of the considered surrounding normal organs were under radiation exposure, and close organs to the liver received a higher dose than the others.

Our findings demonstrated that the dose of secondary particles including photons and neutrons in the non-involved organs, during the liver cancer proton therapy, was minimal. However, the absorbed dose of secondary particles was lower than for the primary particles, the impact of secondary particles should not be ignored which for the precise quantification of the induced secondary cancer after the proton therapy related to the created secondary particles, greater epidemiologic studies are required. Proton therapy procedures can be premeditated in which to localize the position of the Bragg peaks inside the tumor region. Hence, due to the small contribution of the absorbed dose in non-target healthy tissues, relevant side effects and secondary cancer risks of proton therapy may be decreased.

Conflict of Interest

The authors declare no potential conflict of interest regarding the publication of this work.

References

Ahmadi Ganjeh, Z., Eslami-Kalantari, M., and Mowlavi, A. A. (2019). Dosimetry calculations of involved and noninvolved organs in proton therapy of liver cancer: a simulation study. *Nuclear Science and Techniques*, 30:1–7.

Bray, F., Ferlay, J., Soerjomataram, I., et al. (2018). Global cancer statistics 2018: GLOBOCAN estimates of incidence and mortality worldwide for 36 cancers in 185 countries. *CA: a cancer journal for clinicians*, 68(6):394–424.

Brenner, D. J., Elliston, C. D., Hall, E. J., et al. (2009). Reduction of the secondary neutron dose in passively scattered proton radiotherapy, using an optimized pre-collimator/collimator. *Physics in Medicine & Biology*, 54(20):6065.

Brenner, D. J. and Hall, E. J. (2008). Secondary neutrons in clinical proton radiotherapy: a charged issue. *Radiotherapy and Oncology*, 86(2):165–170.

Chen, Y., Grassberger, C., Li, J., et al. (2018). Impact of potentially variable RBE in liver proton therapy. *Physics in Medicine & Biology*, 63(19):195001.

Chuong, M., Kaiser, A., Molitoris, J., et al. (2020). Proton beam therapy for liver cancers. *Journal of Gastrointestinal Oncology*, 11(1):157.

Dionisi, F., Brolese, A., Siniscalchi, B., et al. (2021). Clinical results of active scanning proton therapy for primary liver tumors. *Tumori Journal*, 107(1):71–79.

Doyen, J., Falk, A. T., Floquet, V., et al. (2016). Proton beams in cancer treatments: Clinical outcomes and dosimetric comparisons with photon therapy. *Cancer Treatment Reviews*, 43:104–112.

Gandhi, S. J., Liang, X., Ding, X., et al. (2015). Clinical decision tool for optimal delivery of liver stereotactic body radiation therapy: Photons versus protons. *Practical Radiation Oncology*, 5(4):209–218.

Hälg, R. A. and Schneider, U. (2020). Neutron dose and its measurement in proton therapycurrent state of knowledge. *The British Journal of Radiology*, 93(1107):20190412.

Hashemi, Z., Tatari, M., and Naik, H. (2020). Simulation of dose distribution and secondary particle production in proton therapy of brain tumor. *Reports of Practical Oncology & Radiotherapy*, 25(6):927–933.

Howell, R. (2012). Second primary cancers and cardiovascular disease after radiation therapy. NCRP report no. 170. *Medical Physics*, 39(12):7729–7731.

Jarlskog, C. Z., Lee, C., Bolch, W. E., et al. (2008). Assessment of organ-specific neutron equivalent doses in proton therapy using computational whole-body age-dependent voxel phantoms. *Physics in Medicine & Biology*, 53(3):693.

Jia, S. B., Hadizadeh, M. H., Mowlavi, A. A., et al. (2014). Evaluation of energy deposition and secondary particle production in proton therapy of brain using a slab head phantom. *Reports of Practical Oncology and Radiotherapy*, 19(6):376–384.

Jiang, H., Wang, B., Xu, X. G., et al. (2005). Simulation of organ-specific patient effective dose due to secondary neutrons in proton radiation treatment. *Physics in Medicine & Biology*, 50(18):4337.

Keane, F. K., Wo, J. Y., Zhu, A. X., et al. (2016). Liver-directed radiotherapy for hepatocellular carcinoma. *Liver Cancer*, 5(3):198–209.

Kraft, G. (2000). Tumor therapy with heavy charged particles. *Progress in particle and Nuclear Physics*, 45:S473–S544.

Kry, S. F., Bednarz, B., Howell, R. M., et al. (2017). AAPM TG 158: measurement and calculation of doses outside the treated volume from external-beam radiation therapy. *Medical Physics*, 44(10):e391–e429.

Malmer, C. J. (2001). ICRU report 63. nuclear data for neutron and proton radiotherapy and for radiation protection. *Medical Physics*, 28(5):861.

Paganetti, H. (2002). Nuclear interactions in proton therapy: dose and relative biological effect distributions originating from primary and secondary particles. *Physics in Medicine & Biology*, 47(5):747.

Polf, J., Peterson, S., McCleskey, M., et al. (2009). Measurement and calculation of characteristic prompt gamma ray spectra emitted during proton irradiation. *Physics in Medicine & Biology*, 54(22):N519.

Snyder, W. S., Ford, M. R., Warner, G. G., et al. (1969). Estimates of absorbed fractions for monoenergetic photon sources uniformly distributed in various organs of a heterogeneous phantom. Technical report, Oak Ridge National Lab., Tenn.

Taddei, P. J., Mirkovic, D., Fontenot, J. D., et al. (2009). Stray radiation dose and second cancer risk for a pediatric patient receiving craniospinal irradiation with proton beams. *Physics in Medicine & Biology*, 54(8):2259.

Wang, X., Krishnan, S., Zhang, X., et al. (2008). Proton radiotherapy for liver tumors: dosimetric advantages over photon plans. *Medical Dosimetry*, 33(4):259–267.

Xu, X. G., Bednarz, B., and Paganetti, H. (2008). A review of dosimetry studies on external-beam radiation treatment with respect to second cancer induction. *Physics in Medicine & Biology*, 53(13):R193.

Zheng, Y., Liu, Y., Zeidan, O., et al. (2012). Measurements of neutron dose equivalent for a proton therapy center using uniform scanning proton beams. *Medical Physics*, 39(6Part1):3484–3492.

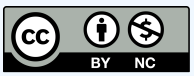

To cite this article:

Mogheiseh, L., Mowlavi, A. A., Jia, S. B., & Shamsabadi, R. (2023). Secondary particle dose assessment during the proton therapy of liver cancer: A Monte Carlo study. *Radiation Physics and Engineering*, 4(3), 65-72.

DOI: 10.22034/rpe.2023.391186.1126

To link to this article: https://doi.org/10.22034/rpe.2023.391186.1126